THE JOURNAL OF PHYSICAL CHEMISTRY C

Article

Cite This: J. Phys. Chem. C 2018, 122, 7951−7958

pubs.acs.org/JPCC

Formation of CO_2 Hydrates within Single-Walled Carbon Nanotubes at Ambient Pressure: CO_2 Capture and Selective Separation of a CO_2/H_2 Mixture in Water

Wenhui Zhao,*[,†] Jaeil Bai,[‡] Joseph S. Francisco,[‡] and Xiao Cheng Zeng*[,‡,§]

[†]Department of Physics, Ningbo University, Ningbo 315211, China

[‡]Department of Chemistry and [§]Department of Chemical & Biomolecular Engineering and Department of Mechanical & Materials Engineering, University of Nebraska-Lincoln, Lincoln, Nebraska 68588, United States

Supporting Information

ABSTRACT: Carbon dioxide (CO_2) capture and separation are two currently accepted strategies to mitigate increasing CO_2 emissions into the atmosphere due to the burning of fossil fuels. Here, we show the simulation results of hydrate-based CO_2 capture and selective separation from the CO_2/H_2 mixture dissolved in water, both using single-walled carbon nanotubes (SW-CNTs). The spontaneous formation of quasi-one-dimensional (Q1D) polygonal CO_2 hydrates under ambient pressure was observed within SW-CNTs immersed in CO_2 aqueous solution. Moreover, highly selective adsorption of a CO_2 over a H_2 molecule is observed in the Q1D polygonal ice nanotube due to a much lower value of the potential mean force (PMF) difference for a CO_2 molecule than for a H_2 molecule enclosed in the corresponding hydrate. The simulation results indicate that the formation of Q1D hydrates can be an effective approach for CO_2 capture or for the separation of CO_2 from H_2 in the mixture.

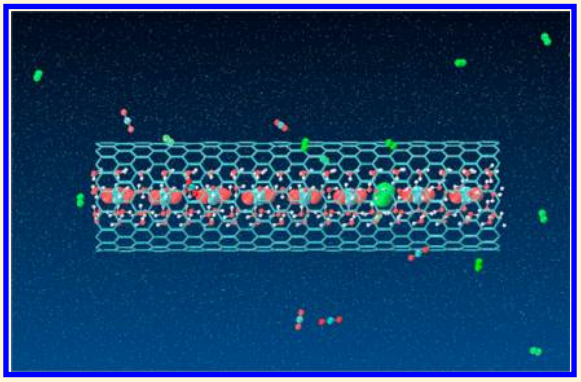

INTRODUCTION

The reduction of carbon dioxide (CO_2) emissions is one of the grand challenges of the 21st century because the fast-increasing concentration of CO_2 (one of the main greenhouse gases) in the atmosphere has led to several significant environmental issues, such as the melting of the polar ice caps, rising sea levels, and climate change. Recently, the 13th World Meteorological Organization (WMO) Global Atmosphere Watch (GAW) annual Greenhouse Gas (GHG) bulletin reported that the CO_2 concentration reached new highs in 2016 (403.3 ± 0.1 ppm), and the record increase was larger than the average growth rate over the past decade.[1] Although several technologies and processes for CO_2 capture, storage, and utilization have been developed,[2−20] more efforts are still needed to halt the growing CO_2 concentration in the atmosphere.

The fast increase in CO_2 concentration is primarily due to the enormous consumption of fossil fuels, e.g., coal, oil, and natural gas. Therefore, one of the possible solutions is to use renewable H_2 as an alternative energy source. However, to date, more than 95% of H_2 used in industry is produced through steam-methane reformation and a subsequent water−gas shift reaction. The effluent gas typically consists of 71−75% H_2, 15−20% CO_2, 4−7% CH_4, 1−4% CO, and other gases such as H_2O.[21] Thus, CO_2 capture and separation from the mixed CO_2 and H_2 gases is required at the least to prevent the release of the CO_2 produced from steam-methane reformation into the atmosphere.

Recently, porous material membranes such as metal-organic frameworks (MOFs) and covalent-organic frameworks (COFs) have demonstrated effective gas-separation capabilities and thus have been recognized as promising media for practical gas adsorption and separation, particularly for CO_2 capture.[22−25] Also, carbon nanomaterials, such as porous graphene and carbon nanotubes (CNTs), have been proposed as promising candidates for gas separation, particularly for H_2 purification.[26−33] However, membrane-based gas separation has to compromise between high permeability and high selectivity.

Hydrate-based technology has been considered to be another promising technology for gas capture and separation besides the conventional technologies (e.g., absorption, adsorption, and membranes) because of its relatively low cost and simple operation.[34] Clathrate hydrates are well-known crystalline inclusion compounds formed by the enclathration of guest species into cages of host-ice frameworks under certain temperature and pressure conditions.[35] The selective capture of guest molecules in the clathrate hydrates offers the possibility of effective gas separation because the conditions for the

Received: December 26, 2017
Revised: February 10, 2018
Published: March 19, 2018

DOI: 10.1021/acs.jpcc.7b12700
J. Phys. Chem. C 2018, 122, 7951−7958

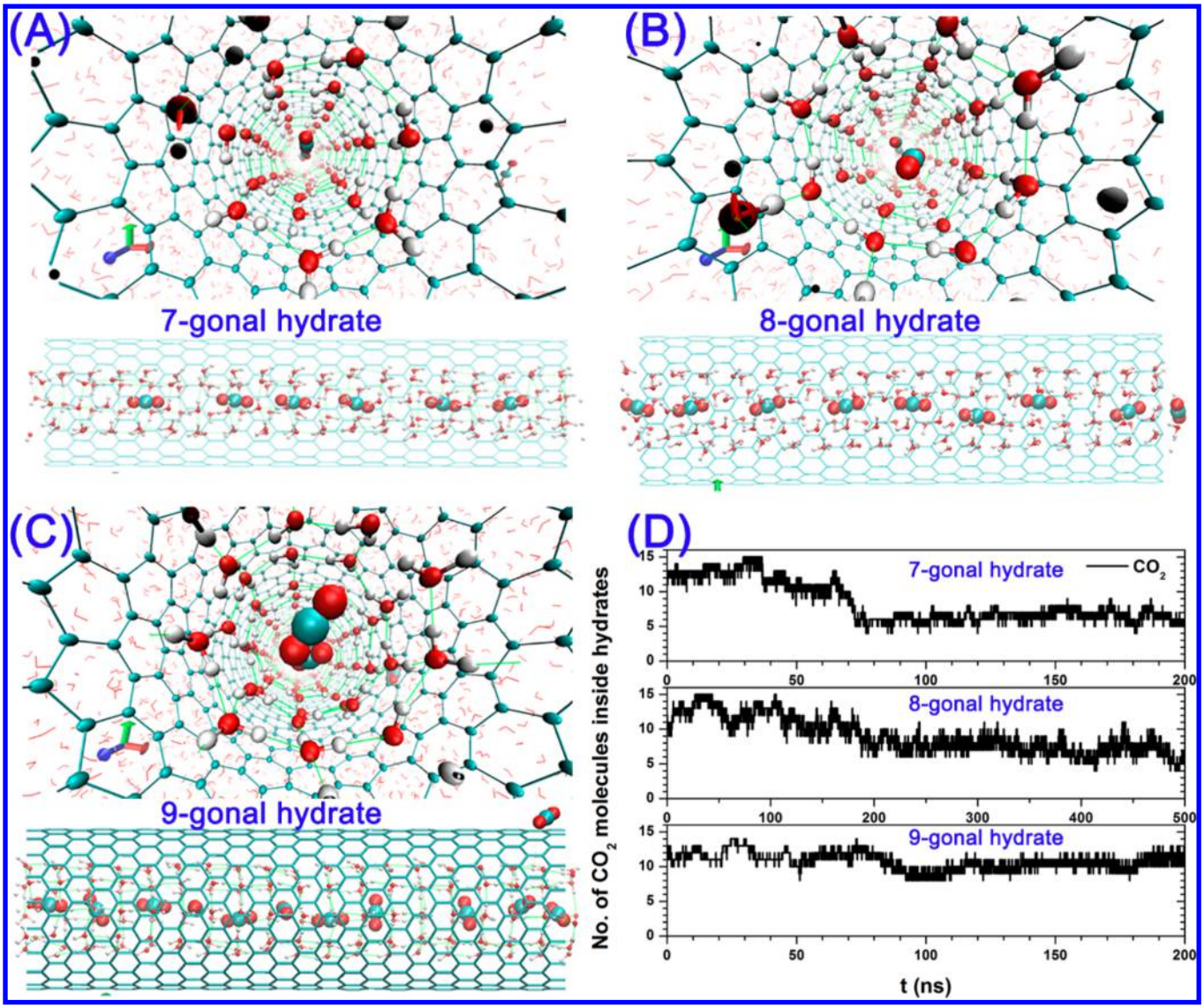

Figure 1. Axial views (top panels) and side views (bottom panels) of the snapshots of the Q1D (A) heptagonal, (B) octagonal, and (C) nonagonal CO_2 hydrates in SW-CNTs. (D) Number of CO_2 molecules within SW-CNTs during the formation of 7-gonal, 8-gonal, and 9-gonal hydrates. Large cyan and red spheres represent the carbon and oxygen atoms of CO_2 molecules, small cyan spheres represent the carbon atoms of SW-CNTs, small red and white spheres represent the oxygen and hydrogen atoms of water confined in SW-CNTs, red lines represent water outside of SW-CNTs (i.e., aqueous solution), and green dotted lines represent hydrogen bonds.

formation of the clathrate hydrates are strongly affected by the guest species to be encaged.[34,36−44] However, the development of hydrate-based CO_2 separation technology is still hampered by the slow growth rate and low selectivity during the hydrate formation process. Numerous investigations suggest that the use of additives can enhance the hydrate formation kinetics and selectivity.[45−51]

Gas hydrate formations in porous media are widespread phenomena in nature. Previous investigations showed that microscale confinement and surface features have both promotion and inhibition effects on the gas hydrate nucleation and growth.[52−61] For example, microscale confinement and the hydrophilic surface of graphene oxide inhibit the hydrate phase,[58] while Casco et al. found that the confinement and hydrophobic surface of carbon cavities can increase the methane hydrate formation rate and lower the hydrate nucleation pressures (below 4 MPa).[59]

When the pore size is reduced to subnanometer levels, the hydrogen-bonding network in water is disrupted by the highly confined environment, thereby affecting the kinetics of crystallization.[62−70] Our previous studies showed that thousands of atmospheric pressures are needed to form monolayer or bilayer gas clathrates within 2D nanoslits,[68−71] whereas quasi-one-dimensional (Q1D) core−sheath polygonal hydrogen and CO hydrates can be formed spontaneously within single-walled carbon nanotubes (SW-CNTs) under ambient pressure.[72,73] More interestingly, the highly preferential adsorption of CO over H_2 is observed in Q1D hydrates within SW-CNTs.[73] Can the Q1D CO_2 hydrates be formed spontaneously in SW-CNTs under ambient pressure, and can the selective adsorption of CO_2 over H_2 (for the mixture dissolved in water) occur within the Q1D hydrates? In this work, we have performed systematic studies to address both questions. The studies can also improve our understanding of different gas clathrates inside a nanoconfined space. By means

DOI: 10.1021/acs.jpcc.7b12700
J. Phys. Chem. C 2018, 122, 7951−7958

of molecular dynamics (MD) simulations, we find that the Q1D heptagonal, octagonal, and nonagonal CO_2 hydrates can be formed spontaneously within SW-CNTs under ambient pressure. More interestingly, highly preferential adsorption of CO_2 over H_2 is also observed within the polygonal hydrates near ambient conditions.

MODEL AND COMPUTATIONAL METHODS

The classical MD simulations are carried out by using the Gromacs 4.5 software[74] package to study the formation of Q1D clathrate hydrates within SW-CNTs, where the SW-CNTs with two open ends are immersed in the dilute CO_2 (or CO_2/H_2) aqueous solution. Three zigzag SW-CNTs with indexes (17, 0), (18, 0), and (19, 0) (whose diameters are 1.33, 1.41, and 1.49 nm, respectively) are considered as our previous studies showed that under ambient pressure the guest-free clathrates can be formed in SW-CNTs with smaller diameters (only a few gas molecules occupy the nanochannels of ice nanotubes), while no clathrates were observed in SW-CNTs with larger diameters.[73] Also, the (10, 10) and (12, 9) SW-CNTs with diameters of 1.356 and 1.429 nm are considered to study the effect of chirality on SW-CNTs. The parameters of SW-CNTs, H_2O, and H_2 molecules are also similar to those used in our previous study,[73] while the CO_2 molecule is treated using the EPM2 model.[75] All MD simulations are carried out with the *NPT* ensemble for 10−500 ns, depending on temperature T and the hydrate formation process. (A detailed simulation description is given in the Supporting Information).

RESULTS AND DISCUSSION

First, the system with the SW-CNTs immersed in a dilute aqueous CO_2 solution is initially equilibrated at 300 K and 1 bar, followed by stepwise cooling in temperature steps of 10 K at ambient pressure. We observed the spontaneous formation of Q1D heptagonal and octagonal CO_2 hydrates in (17, 0) and (18, 0) SW-CNTs, respectively, at 260 K and the formation of a nonagonal CO_2 hydrate in (19, 0) SW-CNT at 240 K. As shown in Figure 1A−C, CO_2 molecules are entrapped within the interior space of the polygonal ice nanotubes and form a single-file wire, akin to the formation of polygonal CO hydrates in the same SW-CNTs.[73] Importantly, as shown in Figure 1D, a heptagonal ice nanotube allows, on average, ∼6.8 CO_2 molecules per supercell to form the heptagonal CO_2 hydrate in (17, 0) SW-CNT. Hence, many more CO_2 molecules are trapped in the heptagonal nanochannel of the ice nanotube than CO (∼1.8) or H_2 (∼3.0) molecules.[73] There are ∼7.1 CO_2, ∼7.8 CO, or ∼7.6 H_2 molecules[73] trapped in the filled octagonal CO_2, CO, or H_2 hydrate within (18, 0) SW-CNT, respectively, and there are ∼10.5 CO_2, ∼9.08 CO, or ∼10.2 H_2 molecules,[73] respectively, contained in the filled nonagonal CO_2, CO, or H_2 hydrates in (19, 0) SW-CNT. In other words, equal numbers of CO_2, CO, or H_2 molecules can be enclosed within the octagonal (and nonagonal) hydrates. The calculated CO_2 weight storage efficiencies for heptagonal, octagonal, and nonagonal hydrates within (17, 0), (18, 0), and (19, 0) SW-CNTs are about 2.43, 2.36, and 3.23%, respectively.

To understand the capturing capability of Q1D polygonal hydrates in SW-CNTs, we first examined the trajectory of CO_2 molecules in hydrates (Figures 2 and S1). Figures 2 and S1 show the motions $z(t)$ of all of the individual CO_2 molecules along the nanotube axis. All of the CO_2 molecules in the Q1D hydrate formed a single-file chain so that they moved

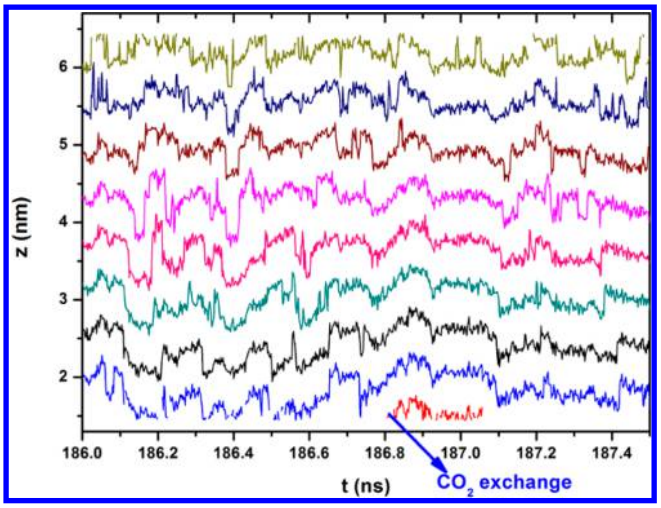

Figure 2. Motions $z(t)$ of individual CO_2 molecules along the nanotube axis shown as colored lines inside the nanochannel of the Q1D heptagonal CO_2 hydrate.

coherently. Most CO_2 molecules oscillate near their equilibrium positions along the z axis. Also, the denser curves indicate more of the CO_2 molecules in the hydrate. Thus, the axial CO_2 density increases with increasing nanotube diameter. Also, we noted that the highest and lowest curves (i.e., at the ends of the CNT) are discontinuous. The discontinuity of the curves indicates that CO_2 molecules exit or enter the hydrate in SW-CNTs. Hence, the CO_2 exchange at the open ends of nanotubes can be observed.

To gain more insight into the polygonal hydrates, we computed the CO_2 molecular orientation and axial density profiles within the hydrates (Figure 3A,B). Here, we define θ as the angle between the CO_2 molecular axis and the positive direction of the z axis (tube axis). As shown in Figure 3A, this orientation is mainly located at 9°, indicating that the CO_2 molecules in a heptagonal hydrate are likely to stay along the hydrate axis, consistent with the single-file structure of CO_2 molecules within the heptagonal hydrate. With the increase in the nanotube diameter (i.e., Q1D hydrate channel diameter), the CO_2 molecular axis deviates from the z axis (Q1D hydrate axis). The deviation can also be observed from the site−site axial distribution functions (ADF) of the CO_2 molecules (Figure 3B). In the heptagonal hydrate (Figure 3B), the first peak of the carbon (C)−carbon (C) ADF (the center atom of CO_2 molecules) is located at ∼0.55 nm, indicating a CO_2 molecule every 0.55 nm length along the z axis. The first and second peaks of the carbon (C)−oxygen (O) ADF are located at ∼0.44 and ∼0.67 nm, suggesting that the CO_2 molecule stays along the tube axis due to the nearly equal distance of the CO_2 oxygen atoms along the z axis in the hydrate (∼0.23 nm) and the length of a free CO_2 (about 0.23 nm). Note that the second peak of C−C ADF is located at ∼0.84 nm, and this peak value is much lower than those of the first and third peaks. This is not an indication of the next-nearest neighbor but of the nearest neighbor with a large distance (i.e., vacancy). The results are consistent with the snapshot of the heptagonal hydrate (Figure 1A). With increasing nanotube diameter (i.e., Q1D hydrate channel diameter), the distance of the nearest neighbor of the CO_2 molecule becomes smaller (about 0.52 nm for the octagonal hydrate and 0.40 nm for the nonagonal hydrate), suggesting that the axial CO_2 density increases. Also, rapidly decaying peaks and the shrinking distance of the first and

DOI: 10.1021/acs.jpcc.7b12700
J. Phys. Chem. C 2018, 122, 7951−7958

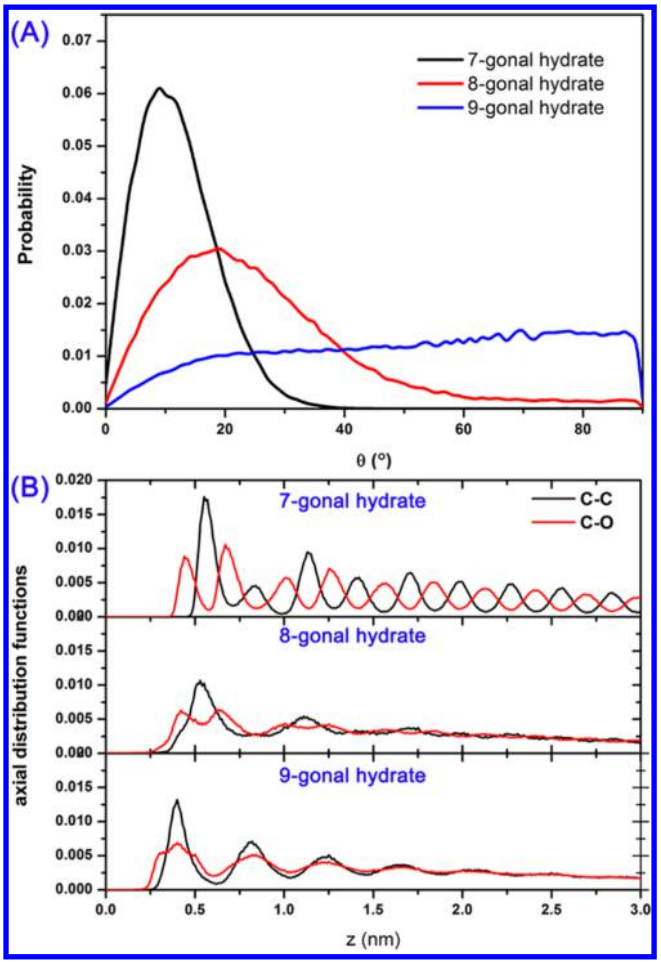

Figure 3. (A) Orientation distribution of CO_2 within Q1D hydrates. (B) Axial distribution functions (ADF) of CO_2 molecules within Q1D hydrates.

second peaks of C−O ADFs for octagonal and nonagonal hydrates indicate that the CO_2 molecular axis deviates from the z axis, consistent with the snapshots of the hydrates (Figure 1B,C) and the CO_2 molecular orientation (Figure 3A).

Next, we studied the systems with the SW-CNTs immersed in a dilute CO_2/H_2 aqueous solution at ambient pressure. Similar to the dilute CO_2 aqueous solution, Q1D heptagonal and octagonal hydrates are formed spontaneously in (17, 0) and (18, 0) SW-CNTs at 260 K, while the formation of the nonagonal hydrate is observed in a (19, 0) SW-CNT at 240 K. Note that many CO_2 molecules and few H_2 molecules are trapped in the Q1D polygonal hydrates (Movies S1 and S2 and Figure 4). Also, importantly, the heptagonal hydrate in (17,0) SW-CNT contains, on average, about 6.4 CO_2 and 1.1 H_2 molecules, respectively (Figure 5A). Thus, the ratio of CO_2/H_2 trapped within the heptagonal hydrate is about 5.8. The number of CO_2 molecules in the hydrate fluctuates between 5 and 9 in the course of the MD simulation, while for most of the time, the number of H_2 molecules fluctuates between 0 and 2. It appears that the Q1D heptagonal hydrate can entail high efficiency to separate the CO_2 and H_2 molecules in dilute CO_2/H_2 aqueous solution, contrary to the dilute CO/H_2 aqueous solution.[73] For the octagonal hydrate in (18, 0) SW-CNT, the average number of CO_2 molecules is about 7.7, while that of the H_2 molecules is only 0.7 (Figure 5B). As a result, the ratio of CO_2/H_2 for the octagonal hydrate is about 11. Therefore, the

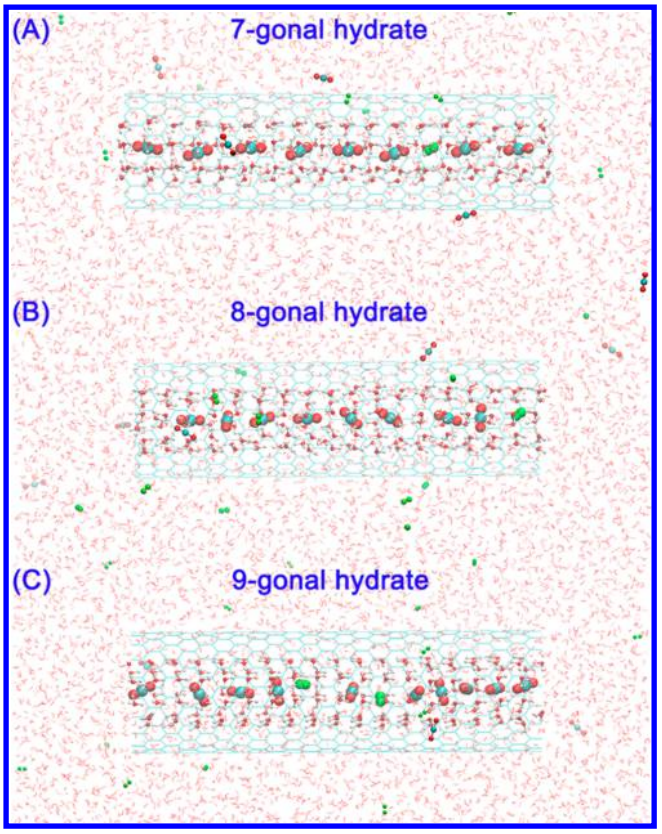

Figure 4. Snapshots of the Q1D (A) heptagonal, (B) octagonal, and (C) nonagonal hydrate in SW-CNTs. Large cyan and red spheres represent the carbon and oxygen atoms of CO_2 molecules in the hydrate, small cyan and red spheres represent the carbon and oxygen atoms of CO_2 molecules outside of the hydrate. Very small cyan spheres represent the carbon atoms of SW-CNTs, large green spheres represent the hydrogen atoms of H_2 molecules in the hydrate, small green spheres represent the hydrogen atoms of H_2 molecules outside of the hydrate, small red and white spheres represent the oxygen and hydrogen atoms of water confined in SW-CNTs, and red lines represent water outside of SW-CNTs (i.e., aqueous solution).

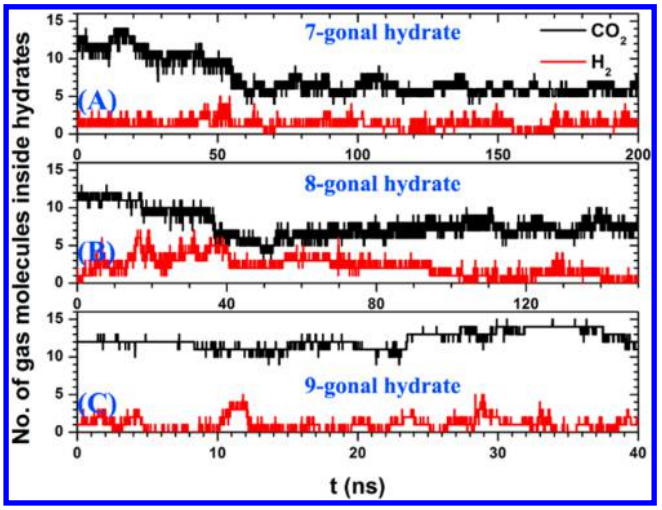

Figure 5. Number of CO_2 and H_2 molecules within SW-CNTs during the formation of (A) 7-gonal, (B) 8-gonal, and (C) 9-gonal hydrates.

Q1D octagonal hydrate can entail higher efficiency to separate the CO_2 and H_2 molecules in a dilute CO_2/H_2 aqueous solution as well. In (19, 0) SW-CNT, the mean number of CO_2

DOI: 10.1021/acs.jpcc.7b12700
J. Phys. Chem. C 2018, 122, 7951−7958

molecules within the nonagonal nanochannel is about 12.3, whereas that of the H_2 molecules is only 0.8 (Figure 5C). The ratio of CO_2/H_2 for the nonagonal hydrate is about 15. Hence, the nonagonal hydrate may entail much higher efficiency to separate the CO_2 and H_2 molecules in a dilute CO_2/H_2 aqueous solution.

To understand the high selective adsorption of CO_2 over H_2 in Q1D hydrates, we computed the potential of mean force (PMF), that is, the free-energy profile, for a gas molecule moving from the bulk solution into the polygonal ice nanotube. (Detailed simulation description is given in the Supporting Information.) As shown in Figure 6, the PMF profiles for the heptagonal hydrate in the (17, 0) SW-CNT show that the energy barriers for CO_2 and H_2 molecules are about −13.9 and −4.5 kJ/mol, respectively. The PMF profiles for the octagonal hydrate in the (18, 0) SW-CNT show that the PMF difference for a CO_2 molecule is about −14.8 kJ/mol and that of a H_2 molecule is ∼−7.5 kJ/mol. For the nonagonal hydrate in the (19, 0) SW-CNT, the energy barrier for a CO_2 molecule is about −11.5 kJ/mol, and that of a H_2 molecule is ∼−5.2 kJ/mol. The negative values of the PMF barriers for CO_2 and H_2 molecules indicate that both molecules would prefer to enter the nanochannels of the Q1D polygonal hydrates within SW-CNTs. More importantly, the much more negative value of the PMF difference for a CO_2 molecule indicates that a CO_2 molecule is more preferred over a H_2 molecule to be adsorbed in the hydrate.

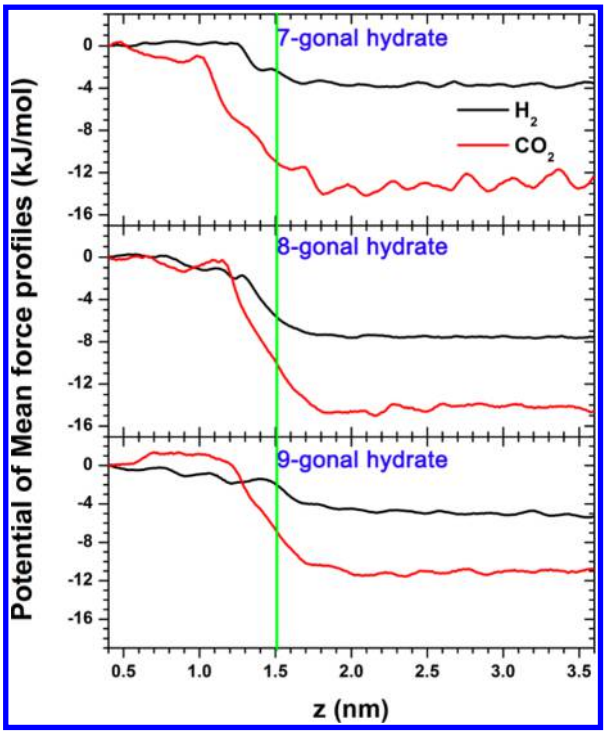

Figure 6. Potential of mean force (PMF) profiles for H_2 and CO_2 molecules within the polygonal ice nanotubes. The green line represents the end of the SW-CNTs.

To study the effect of the CNTs' chirality on hydrate formation and the high selectivity of CO_2 over H_2, we carried out additional MD simulations with (10, 10) and (12, 9) SW-CNTs immersed in the dilute CO_2 (or CO_2/H_2) aqueous solution. By decreasing the temperature, the helical and octagonal hydrates are formed spontaneously within (10, 10) and (12, 9) SW-CNTs, respectively. Also, importantly, the highly selective adsorption of CO_2 over H_2 in the hydrates was observed (Figure 7). The formation of 1D gas hydrates within CNTs and the high selectivity of CO_2 over H_2 are dependent on the SW-CNTs' diameter rather than their chirality, as in the case of the formation of the Q1D polygonal ice nanotube in SW-CNTs.[64]

We also carried out additional MD simulations to demonstrate that the solubility of CNTs in water does not affect the formation of 1D gas hydrates within CNTs and the high selectivity of CO_2 over H_2. Here, the SW-CNT membrane composed of (18, 0) SW-CNTs combined with two opposing graphene sheets is used to separate the gas aqueous solution. The spontaneous formation of the octagonal hydrate in the CNT membrane and the high selectivity of CO_2 over H_2 in the hydrate were observed as well (Figure 8 and Movie S4).

We performed the latest MD simulations to study the stability of the Q1D hydrates under a gas atmosphere. In the simulation system, many water molecules are removed, and a few of the water molecules are adsorbed near the ends of

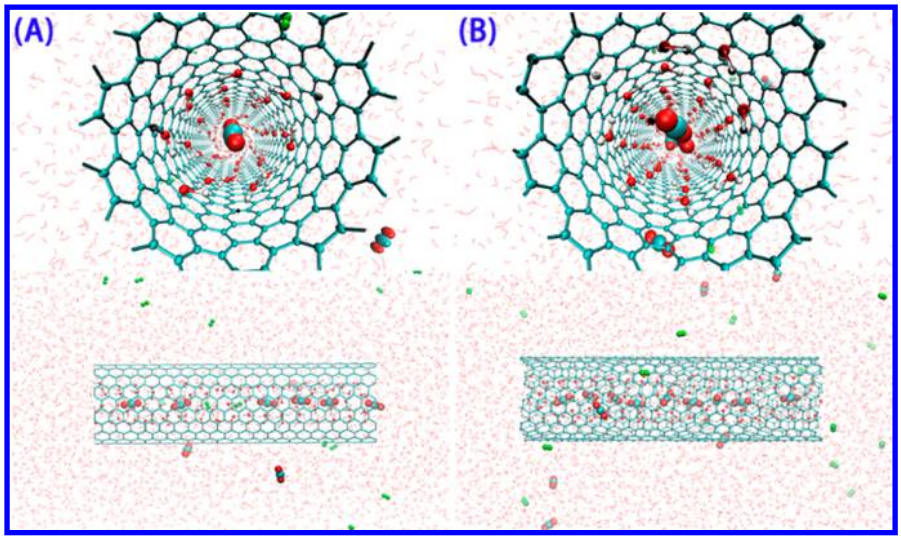

Figure 7. Axial views (top panels) and side views (bottom panels) of the snapshots of the Q1D (A) helical and (B) octagonal hydrates in (10, 10) and (12, 9) SW-CNTs at 260 K.

DOI: 10.1021/acs.jpcc.7b12700
J. Phys. Chem. C 2018, 122, 7951−7958

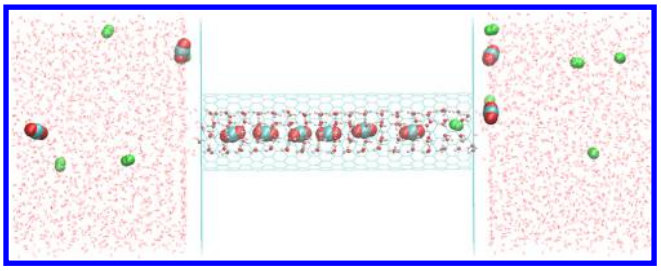

Figure 8. Snapshot of the octagonal hydrate in the SW-CNT membrane.

CNTs. The results show that the Q1D hydrates in SW-CNTs are stable (Figure 9 and Movies S5 and S6).

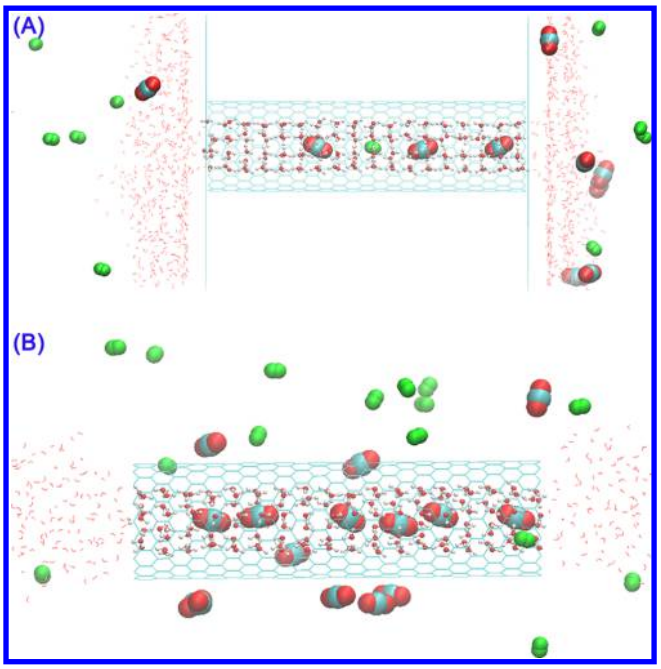

Figure 9. Snapshots of the hydrate within the SW-CNTs under a gas atmosphere.

CONCLUSIONS

We have presented simulation evidence of the spontaneous formation of Q1D polygonal (7-, 8-, and 9-gonal) CO_2 hydrates within SW-CNTs under ambient pressure for SW-CNTs immersed in a dilute CO_2 aqueous solution. The polygonal CO_2 hydrates are very similar to the polygonal H_2 and CO hydrates previously reported.[73] More interestingly, the highly selective adsorption of a CO_2 over a H_2 molecule is observed within the Q1D polygonal hydrates due to the much lower value of the PMF difference for a CO_2 molecule compared to that of a H_2 molecule to be trapped in the hydrates. Also, our results show that the formation of 1D gas hydrates within CNTs and the high selectivity of CO_2 over H_2 are dependent on the SW-CNTs' diameter rather than their chirality, as in the case of the formation of the Q1D polygonal ice nanotube in SW-CNTs.[64] Note that our previous study also showed the high preferential adsorption of a CO over a H_2 molecule in the Q1D polygonal hydrates.[73] Hence, the formation of Q1D hydrates may be a useful approach for the capture of CO_2 and for the removal of CO_2 and CO from H_2, particularly for hydrogen purification from the syngas in fuel-cell devices.

ASSOCIATED CONTENT

Supporting Information

The material is available free of charge via the Internet at The Supporting Information is available free of charge on the ACS Publications website at DOI: 10.1021/acs.jpcc.7b12700.

Computational details and calculations (PDF)
Molecular dynamics simulation trajectories of Q1D hydrates formed in the SW-CNTs (MPG)
Molecular dynamics simulation trajectories of Q1D hydrates formed in the SW-CNTs (MPG)
Molecular dynamics simulation trajectories of Q1D hydrates formed in the SW-CNTs (MPG)
Molecular dynamics simulation trajectories of Q1D hydrates formed in the SW-CNTs (MPG)
Molecular dynamics simulation trajectories of Q1D hydrates formed in the SW-CNTs (MPG)
Molecular dynamics simulation trajectories of Q1D hydrates formed in the SW-CNTs (MPG)

AUTHOR INFORMATION

Corresponding Authors

*E-mail: zhaowenhui@nbu.edu.cn.
*E-mail: xzeng1@unl.edu.

ORCID

Joseph S. Francisco: 0000-0002-5461-1486
Xiao Cheng Zeng: 0000-0003-4672-8585

Notes

The authors declare no competing financial interest.

ACKNOWLEDGMENTS

We thank UNL Holland Computing Center for offering CPU time. W.Z. is supported by the National Natural Science Foundation of China (21503205), Zhejiang Provincial Natural Science Foundation of China (LY18B030003), Anhui Provincial Natural Science Foundation (1608085QB30), and the K. C. Wong Magna Fund in Ningbo University. J.S.F., X.C.Z., and J.B. are supported by U.S. NSF (grant no. CHE-1665324).

REFERENCES

(1) WMO Greenhouse Gas Bulletin No. 13: http://www.wmo.int/pages/prog/arep/gaw/ghg/ghg-bulletin13.htm, accessed Oct 30, 2017.
(2) Rochelle, G. T. Amine Scrubbing for CO_2 Capture. *Science* **2009**, *325*, 1652−1654.
(3) Haszeldine, R. S. Carbon Capture and Storage: How Green Can Black Be? *Science* **2009**, *325*, 1647−1652.
(4) Sumida, K.; Rogow, D. L.; Mason, J. A.; McDonald, T. M.; Bloch, E. D.; Herm, Z. R.; Bae, T. H.; Long, J. R. Carbon Dioxide Capture in Metal-Organic Frameworks. *Chem. Rev.* **2012**, *112*, 724−781.
(5) Wang, Q.; Luo, J.; Zhong, Z.; Borgna, A. CO_2 Capture by Solid Adsorbents and Their Applications: Current Status and New Trends. *Energy Environ. Sci.* **2011**, *4*, 42−55.
(6) Du, N. Y.; Park, H. B.; Robertson, G. P.; Dal-Cin, M. M.; Visser, T.; Scoles, L.; Guiver, M. D. Polymer Nanosieve Membranes for CO_2-Capture Applications. *Nat. Mater.* **2011**, *10*, 372−375.
(7) Bhown, A. S.; Freeman, B. C. Analysis and Status of Post-Combustion Carbon Dioxide Capture Technologies. *Environ. Sci. Technol.* **2011**, *45*, 8624−8632.
(8) Yuan, Z.; Eden, M. R.; Gani, R. Toward the Development and Deployment of Large-Scale Carbon Dioxide Capture and Conversion Processes. *Ind. Eng. Chem. Res.* **2016**, *55*, 3383−3419.
(9) Gao, W.-Y.; Wu, H.; Leng, K.; Sun, Y.; Ma, S. Inserting CO_2 into Aryl C-H Bonds of Metal-Organic Frameworks: CO_2 Utilization for

DOI: 10.1021/acs.jpcc.7b12700
J. Phys. Chem. C 2018, 122, 7951−7958

Direct Heterogeneous C-H Activation. *Angew. Chem., Int. Ed.* **2016**, *55*, 5472−5476.
(10) Creamer, A.; Gao, B. Carbon-Based Adsorbents for Post-combustion CO_2 Capture: A Critical Review. *Environ. Sci. Technol.* **2016**, *50*, 7276−7289.
(11) Wang, J.; Wang, S.; Xin, Q.; Li, Y. Perspectives on Water-Facilitated CO_2 Capture Materials. *J. Mater. Chem. A* **2017**, *5*, 6794−6816.
(12) Nugent, P.; Belmabkhout, Y.; Burd, S. D.; Cairns, A. J.; Luebke, R.; Forrest, K.; Pham, T.; Ma, S.; Space, B.; Wojtas, L.; et al. Porous Materials with Optimal Adsorption Thermodynamics and Kinetics for CO_2 Separation. *Nature* **2013**, *495*, 80−84.
(13) Yu, J.; Xie, L.-H.; Li, J.-R.; Ma, Y.; Seminario, J.; Balbuena, P. CO_2 Capture and Separation Using MOFs: Computational and Experimental Studies. *Chem. Rev.* **2017**, *117*, 9674−9754.
(14) Brennecke, J.; Gurkan, B. Ionic Liquids for CO_2 Capture and Emission Reduction. *J. Phys. Chem. Lett.* **2010**, *1*, 3459−3464.
(15) Zeng, S.; Zhang, X.; Bai, L.; Zhang, X.; Wang, H.; Wang, J.; Bao, D.; Li, M.; Liu, X.; Zhang, S. Ionic-Liquid-Based CO_2 Capture Systems: Structure, Interaction and Process. *Chem. Rev.* **2017**, *117*, 9625−9673.
(16) Wang, Q.; Bai, J.; Lu, Z.; Pan, Y.; You, X. Finely Tuning MOFs towards High-Performance Post-Combustion CO_2 Capture Materials. *Chem. Commun.* **2016**, *52*, 443−452.
(17) Jiang, H.; Economou, I.; Panagiotopoulos, A. Molecular Modeling of Thermodynamic and Transport Properties for CO_2 and Aqueous Brines. *Acc. Chem. Res.* **2017**, *50*, 751−758.
(18) Noiriel, C.; Daval, D. Pore-Scale Geochemical Reactivity Associated with CO_2 Storage: New Frontiers at the Fluid-Solid Interface. *Acc. Chem. Res.* **2017**, *50*, 759−768.
(19) Xia, D.; Xue, Q.; Xie, J.; Chen, H.; Lv, C.; Besenbacher, F.; Dong, M. Fabrication of Carbon Nanoscrolls from Monolayer Graphene. *Small* **2010**, *6*, 2010−2019.
(20) Ma, M.; Hansen, H. A.; Valenti, M.; Wang, Z.; Cao, A.; Dong, M. Electrochemical Reduction of CO_2 on Compositionally Variant Au-Pt Bimetallic Thin Films. *Nano Energy* **2017**, *42*, 51−57.
(21) Hufton, J. R.; Mayorga, S.; Sircar, S. Sorption-Enhanced Reaction Process for Hydrogen Production. *AIChE J.* **1999**, *45*, 248−256.
(22) Fu, J.; Das, S.; Xing, G.; Ben, T.; Valtchev, V.; Qiu, S. Fabrication of COF-MOF Composite Membranes and Their Highly Selective Separation of H_2/CO_2. *J. Am. Chem. Soc.* **2016**, *138*, 7673−7680.
(23) Eddaoudi, M.; Kim, J.; Rosi, N.; Vodak, D.; Wachter, J.; O'Keeffe, M.; Yaghi, O. M. Systematic Design of Pore Size and Functionality in Isoreticular MOFs and Their Application in Methane Storage. *Science* **2002**, *295*, 469−472.
(24) Du, L.; Lu, Z.; Zheng, K.; Wang, J.; Zheng, X.; Pan, Y.; You, X.; Bai, J. Fine-Tuning Pore Size by Shifting Coordination Sites of Ligands and Surface Polarization of Metal-Organic Frameworks to Sharply Enhance the Selectivity for CO_2. *J. Am. Chem. Soc.* **2013**, *135*, 562−565.
(25) Li, J.-R.; Sculley, J.; Zhou, H.-C. Metal-Organic Frameworks for Separations. *Chem. Rev.* **2012**, *112*, 869−932.
(26) Jiang, D.; Cooper, V. R.; Dai, S. Porous Graphene as the Ultimate Membrane for Gas Separation. *Nano Lett.* **2009**, *9*, 4019−4024.
(27) Koenig, S.; Wang, L.; Pellegrino, J.; Bunch, J. Selective Molecular Sieving through Porous Graphene. *Nat. Nanotechnol.* **2012**, *7*, 728−732.
(28) Li, H.; Song, Z.; Zhang, X.; Huang, Y.; Li, S.; Mao, Y.; Ploehn, H.; Bao, Y.; Yu, M. Ultrathin, Molecular-Sieving Graphene Oxide Membranes for Selective Hydrogen Separation. *Science* **2013**, *342*, 95−98.
(29) Jiao, Y.; Du, A.; Smith, S.; Zhu, Z.; Qiao, S. H_2 Purification by Functionalized Graphdiyne-Role of Nitrogen Doping. *J. Mater. Chem. A* **2015**, *3*, 6767−6771.
(30) Shen, J.; Liu, G.; Huang, K.; Chu, Z.; Jin, W.; Xu, N. Subnanometer Two-Dimensional Graphene Oxide Channels for Ultrafast Gas Sieving. *ACS Nano* **2016**, *10*, 3398−3409.
(31) Boutilier, M.; Jang, D.; Idrobo, J.; Kidambi, P.; Hadjiconstantinou, N.; Karnik, R. Molecular Sieving Across Centimeter-Scale Single-Layer Nanoporous Graphene Membranes. *ACS Nano* **2017**, *11*, 5726−5736.
(32) Yuan, Z.; Rajan, A.; Misra, R.; Drahushuk, L.; Agrawal, K.; Strano, M.; Blankschtein, D. Mechanism and Prediction of Gas Permeation through Sub-Nanometer Graphene Pores: Comparison of Theory and Simulation. *ACS Nano* **2017**, *11*, 7974−7987.
(33) Svoboda, M.; Brennan, J. K.; Lisal, M. Molecular Dynamics Simulation of Carbon Dioxide in Single-Walled Carbon Nanotubes in the Presence of Water: Structure and Diffusion Studies. *Mol. Phys.* **2015**, *113*, 1124−1136.
(34) Kang, S.-P.; Lee, H. Recovery of CO_2 from Flue Gas Using Gas Hydrate: Thermodynamic Verification through Phase Equilibrium Measurements. *Environ. Sci. Technol.* **2000**, *34*, 4397−4400.
(35) Sloan, E. D. Fundamental Principles and Applications of Natural Gas Hydrates. *Nature* **2003**, *426*, 353−363.
(36) Yang, Y.; Shin, D.; Choi, S.; Woo, Y.; Lee, J.; Kim, D.; Shin, H.; Cha, M.; Yoon, J. Selective Encaging of N_2O in N_2O-N_2 Binary Gas Hydrates via Hydrate-Based Gas Separation. *Environ. Sci. Technol.* **2017**, *51*, 3550−3557.
(37) Makogon, Y. F.; Holditch, S. A.; Makogon, T. Y. Natural Gas-Hydrates- A Potential Energy Source for the 21st Century. *J. Pet. Sci. Eng.* **2007**, *56*, 14−31.
(38) Orr, F. M., Jr. CO_2 Capture and Storage: Are We Ready? *Energy Environ. Sci.* **2009**, *2*, 449−458.
(39) Zhou, X. T.; Fan, S. S.; Liang, D. Q.; Du, J. W. Replacement of Methane from Quartz Sand-Bearing Hydrate with Carbon Dioxide-in-Water Emulsion. *Energy Fuels* **2008**, *22*, 1759−1764.
(40) Roman-Perez, G.; Moaied, M.; Soler, J. M.; Yndurain, F. Stability, Adsorption, and Diffusion of CH_4, CO_2, and H_2 in Clathrate Hydrates. *Phys. Rev. Lett.* **2010**, *105*, 145901.
(41) Cha, M.; Shin, K.; Lee, H.; Moudrakovski, I. L.; Ripmeester, J. A.; Seo, Y. Kinetics of Methane Hydrate Replacement with Carbon Dioxide and Nitrogen Gas Mixture Using in Situ NMR Spectroscopy. *Environ. Sci. Technol.* **2015**, *49*, 1964−1971.
(42) Birkedal, K. A.; Hauge, L. P.; Graue, A.; Ersland, G. Transport Mechanisms for CO_2-CH_4 Exchange and Safe CO_2 Storage in Hydrate-Bearing Sandstone. *Energies* **2015**, *8*, 4073−4095.
(43) Babu, P.; Linga, P.; Kumar, R.; Englezos, P. A Review of the Hydrate Based Gas Separation (HBGS) Process for Carbon Dioxide Pre-Combustion Capture. *Energy* **2015**, *85*, 261−279.
(44) Mu, L.; Solms, N. Methane Production and Carbon Capture by Hydrate Swapping. *Energy Fuels* **2017**, *31*, 3338−3347.
(45) Fan, S.; Long, X.; Lang, X.; Wang, Y.; Chen, J. CO_2 Capture from CH_4/CO_2 Mixture Gas with Tetra-n-butylammonium Bromide Semi-Clathrate Hydrate through a Pressure Recovery Method. *Energy Fuels* **2016**, *30*, 8529−8534.
(46) Di Profio, P.; Canale, V.; D'Alessandro, N.; Germani, R.; Crescenzo, A.; Fontana, A. Separation of CO_2 and CH_4 from Biogas by Formation of Clathrate Hydrates: Importance of the Driving Force and Kinetic Promoters. *ACS Sustainable Chem. Eng.* **2017**, *5*, 1990−1997.
(47) Ma, Z. W.; Zhang, P.; Bao, H. S.; Deng, S. Review of Fundamental Properties of CO_2 Hydrates and CO_2 Capture and Separation Using Hydration Method. *Renewable Sustainable Energy Rev.* **2016**, *53*, 1273−1302.
(48) Fukumoto, A.; Silva, L.; Paricaud, P.; Dalmazzone, D.; Furst, W. Modeling of the Dissociation Conditions of H_2+CO_2 Semiclathrate Hydrate Formed with TBAB, TBAC, TBAF, TBPB, and $TBNO_3$ Salts. Application to CO_2 Capture from Syngas. *Int. J. Hydrogen Energy* **2015**, *40*, 9254−9266.
(49) Liu, H.; Wang, J.; Chen, G.; Liu, B.; Dandekar, A.; Wang, B.; Zhang, X.; Sun, C.; Ma, Q. High-Efficiency Separation of a CO_2/H_2 Mixture via Hydrate Formation in W/O Emulsions in the Presence of

DOI: 10.1021/acs.jpcc.7b12700
J. Phys. Chem. C 2018, 122, 7951−7958

Cyclopentane and TBAB. *Int. J. Hydrogen Energy* **2014**, *39*, 7910−7918.
(50) Xia, Z.; Li, X.; Chen, Z.; Yan, K.; Xu, C.; Cai, J. Hydrate-Based Hydrogen Purification from Simulated Syngas with Synergic Additives. *Int. J. Hydrogen Energy* **2016**, *41*, 2649−2659.
(51) Nguyen, N.; Nguyen, A. Hydrophobic Effect on Gas Hydrate Formation in the Presence of Additives. *Energy Fuels* **2017**, *31*, 10311−10323.
(52) Kim, D.; Ahn, Y.-H.; Kim, S.-J.; Lee, J. Y.; Lee, J.; Seo, Y.-j.; Lee, H. Gas Hydrate in Crystalline-Swelled Clay: The Effect of Pore Dimension on Hydrate Formation and Phase Equilibria. *J. Phys. Chem. C* **2015**, *119*, 22148−22153.
(53) Lee, S.; Cha, I.; Seo, Y. Phase Behavior and ^{13}C NMR Spectroscopic Analysis of the Mixed Methane + Ethane + Propane Hydrates in Mesoporous Silica Gels. *J. Phys. Chem. B* **2010**, *114*, 15079−15084.
(54) Seo, Y.; Lee, S.; Cha, I.; Lee, J. D.; Lee, H. Phase Equilibria and Thermodynamics Modeling of Ethane and Propane Hydrates in Porous Silica Gels. *J. Phys. Chem. B* **2009**, *113*, 5487−5492.
(55) Seshadri, K.; Wilder, J. W.; Smith, D. H. Measurements of Equilibrium Pressures and Temperatures for Propane Hydrate in Silica Gels with Different Pore-Size Distributions. *J. Phys. Chem. B* **2001**, *105*, 2627−2631.
(56) Yang, M.; Song, Y.; Jiang, L.; Zhu, N.; Liu, Y.; Zhao, Y.; Dou, B.; Li, Q. CO_2 Hydrate Formation and Dissociation in Cooled Porous Media: A Potential Technology for CO_2 Capture and Storage. *Environ. Sci. Technol.* **2013**, *47*, 9739−9746.
(57) Kim, D.; Ahn, Y.-H.; Lee, H. Phase Equilibria of CO_2 and CH_4 Hydrates in Intergranular Meso/Macro Pores of MIL-53 Metal Organic Framework. *J. Chem. Eng. Data* **2015**, *60*, 2178−2185.
(58) Kim, D.; Kim, D. W.; Lim, H.-K.; Jeon, J.; Kim, H.; Jung, H.-T.; Lee, H. Inhibited Phase Behavior of Gas Hydrates in Graphene Oxide: Influences of Surface and Geometric Constraints. *Phys. Chem. Chem. Phys.* **2014**, *16*, 22717−22722.
(59) Casco, M. E.; Silvestre-Albero, J.; Ramírez-Cuesta, A. J.; Rey, F.; Jorda, J. L.; Bansode, A.; Urakawa, A.; Peral, I.; Martínez-Escandell, M.; Kaneko, K.; et al. Methane Hydrate Formation in Confined Nanospace Can Surpass Nature. *Nat. Commun.* **2015**, *6*, 6432.
(60) Casco, M. E.; Jorda, J. L.; Rey, F.; Fauth, F.; Martínez-Escandell, M.; Rodríguez-Reinoso, F.; Ramos-Fernandez, E. V.; Silvestre-Albero, J. High-Performance of Gas Hydrates in Confined Nanospace for Reversible CH_4/CO_2 Storage. *Chem. - Eur. J.* **2016**, *22*, 10028−10035.
(61) Borchardt, L.; Nickel, W.; Casco, M.; Senkovska, I.; Bon, V.; Wallacher, D.; Grimm, N.; Krause, S.; Silvestre-Albero, J. Illuminating Solid Gas Storage in Confined Spaces - Methane Hydrate Formation in Porous Model Carbons. *Phys. Chem. Chem. Phys.* **2016**, *18*, 20607−20614.
(62) Koga, K.; Tanaka, H.; Zeng, X. C. First-Order Transition in Confined Water between High-Density Liquid and Low-Density Amorphous Phases. *Nature* **2000**, *408*, 564−567.
(63) Koga, K.; Gao, G. T.; Tanaka, H.; Zeng, X. C. Formation of Ordered Ice Nanotubes Inside Carbon Nanotubes. *Nature* **2001**, *412*, 802−805.
(64) Takaiwa, D.; Hatano, I.; Koga, K.; Tanaka, H. Phase Diagram of Water in Carbon Nanotubes. *Proc. Natl. Acad. Sci. U. S. A.* **2008**, *105*, 39−43.
(65) Zhao, W.-H.; Bai, J.; Yuan, L.-F.; Yang, J.; Zeng, X. C. Ferroelectric Hexagonal and Rhombic Monolayer Ices. *Chem. Sci.* **2014**, *5*, 1757−1764.
(66) Algara-Siller, G.; Lehtinen, O.; Wang, F. C.; Nair, R. R.; Kaiser, U.; Wu, H. A.; Geim, A. K.; Grigorieva, I. V. Square Ice in Graphene Nanocapillaries. *Nature* **2015**, *519*, 443−445.
(67) Zhu, W.; Zhao, W.-H.; Wang, L.; Yin, D.; Jia, M.; Yang, J.; Zeng, X. C.; Yuan, L.-F. Two-Dimensional Interlocked Pentagonal Bilayer Ice: How Do Water Molecules Form A Hydrogen Bonding Network? *Phys. Chem. Chem. Phys.* **2016**, *18*, 14216−14221.
(68) Bai, J.; Angell, C. A.; Zeng, X. C. Guest-Free Monolayer Clathrate and Its Coexistence with Two-Dimensional High-Density Ice. *Proc. Natl. Acad. Sci. U. S. A.* **2010**, *107*, 5718−5722.
(69) Bai, J.; Zeng, X. C. Polymorphism and Polyamorphism in Bilayer Water Confined to Slit Nanopore under High Pressure. *Proc. Natl. Acad. Sci. U. S. A.* **2012**, *109*, 21240−21245.
(70) Zhao, W.-H.; Wang, L.; Bai, J.; Yuan, L.-F.; Yang, J.; Zeng, X. C. Highly Confined Water: Two-Dimensional Ice, Amorphous Ice, and Clathrate Hydrates. *Acc. Chem. Res.* **2014**, *47*, 2505−2513.
(71) Zhao, W.-H.; Bai, J.; Wang, L.; Yuan, L.-F.; Yang, J.; Francisco, J. S.; Zeng, X. C. Formation of Bilayer Clathrate Hydrates. *J. Mater. Chem. A* **2015**, *3*, 5547−5555.
(72) Zhao, W.-H.; Wang, L.; Bai, J.; Francisco, J. S.; Zeng, X. C. Spontaneous Formation of One-Dimensional Hydrogen Gas Hydrate in Carbon Nanotubes. *J. Am. Chem. Soc.* **2014**, *136*, 10661−10668.
(73) Zhao, W.-H.; Bai, J.; Francisco, J. S.; Zeng, X. C. CO Separation from H_2 via Hydrate Formation in Single-Walled Carbon Nanotubes. *J. Phys. Chem. Lett.* **2016**, *7*, 4911−4915.
(74) Hess, B.; Kutzner, C.; van der Spoel, D.; Lindahl, E. GROMACS 4: Algorithms for Highly Efficient, Load-Balanced, and Scalable Molecular Simulation. *J. Chem. Theory Comput.* **2008**, *4*, 435−447.
(75) Harris, J. G.; Yung, K. H. Carbon Dioxide's Liquid-Vapor Coexistence Curve and Critical Properties as Predicted by a Simple Molecular Model. *J. Phys. Chem.* **1995**, *99*, 12021−12024.

DOI: 10.1021/acs.jpcc.7b12700
J. Phys. Chem. C 2018, 122, 7951−7958